Energy relaxation in edge modes in the quantum Hall effect

Amir Rosenblatt[1], Sofia Konyzheva[1], Fabien Lafont[1], Noam Schiller[1], Jinhong Park[2], Kyrylo Snizhko[1], Moty Heiblum[1], Yuval Oreg[1] and Vladimir Umansky[1]

1. *Braun Center for Submicron Research, Department of Condensed Matter Physics, Weizmann Institute of Science, Rehovot 761001, Israel*

2. *Institute for Theoretical Physics, University of Cologne, Zülpicher Str. 77, 50937 Köln, Germany*

Abstract

Studies of energy flow in quantum systems complement the information provided by common conductance measurements. The quantum limit of heat flow in one dimensional (1D) ballistic modes was predicted, and experimentally demonstrated, to have a universal value for bosons, fermions and fractionally charged anyons. A fraction of this value is expected in non-abelian states. Nevertheless, open questions about energy relaxation along the propagation length in 1D modes remain. Here, we introduce a novel experimental setup that measures the energy relaxation in chiral 1D modes of the quantum Hall effect (QHE). Edge modes, emanating from a heated reservoir, are partitioned by a quantum point contact (QPC) located at their path. The resulting noise allows a determination of the 'effective temperature' at the location of the QPC. We found energy relaxation in all the tested QHE states, being integers or fractional. However, the relaxation was found to be mild in particle-like states, and prominent in hole-conjugate states.

Pendry [1] was the first to predict a universal upper limit of heat conductance in ballistic one-dimensional modes. This limit holds for any modes of abelian particles, and is independent of particles' exchange statistics [2–4]. Indeed, recent experiments confirmed this upper limit of heat flow with photons [5], phonons [6], electrons [7–11], and fractional charges [11,12]. For modes of non-abelian particles, a fractional upper limit of the thermal conductance is expected, and recently measured, in the $\nu = 5/2$ state of the quantum Hall effect (QHE) [12,13]. Moreover, the measured fractional thermal conductance [12] narrowed down the possible topological orders of that non-abelian state [14–24], reveling information that cannot be obtained by the ubiquitous electrical conductance measurements.

A key element, a small floating reservoir (a micron-size ohmic contact) [25], was used in all the experiments that measured the thermal conductance of chiral edge modes in the QHE [9–12,26,27]. The reservoir's temperature is governed by the power dissipated in the reservoir (a balance between the electrical and heat power flowing in and out). A voltage amplifier, located downstream from the floating reservoir, measures the low frequency thermal noise [28,29], thus obtaining the temperature T_m of the reservoir [9–12]. While energy relaxation may occur as the modes propagate, low frequency noise ($hf \ll k_B T_m$, f - frequency, h - Planck constant, k_B - Boltzmann constant) is insensitive to energy relaxation due to current conservation. We use three terms to refer the redistribution of the energy profile: *relaxation* – any redistribution of the energy profile; *equilibration* – a relaxation without energy loss; *dissipation* – relaxation due to energy loss.

A priori, in particle-like states heat flows solely downstream and thus may lose heat only to the environment. However, in electron-hole conjugate states, as well as in non-abelian states, with counter-propagating modes, heat can be exchanged between the downstream and upstream modes, which can lead to temperature gradients along the edge (appearing as energy dissipating along the edge) [3,14,30–33]. Previous studies using quantum dot spectroscopy [34–38] observed energy relaxation at the integer QHE regime; a strong inter-edge equilibration was found as the main relaxation mechanism, while an additional dissipation remains inconclusive [39–41].

In our study, we employ a new method to detect energy relaxation in QHE edge modes. The heated edge modes that emanate from the floating reservoir are partitioned with a partly pinched QPC. The resulting noise provides information of

the energy relaxation at the location of the QPC. A model consisting of low-frequency current conservation accompanied by dissipation [42], is found to be in good agreement with the data. However, as we discuss later, this is not sufficient to rule out energy equilibration without dissipation.

The experimental setup, shown in Fig. 1a, consists of two regions of high mobility two-dimensional electron gas (light grey) embedded in GaAs-AlGaAs heterostructure, with an electron density 0.9×10^{11} cm^{-2} and a mobility of 4.6×10^6 cm^{2}V^{-1}s^{-1} (at 4.2K). The two regions, separated by a narrow etched trench (dark grey), are bridged by a small, floating, ohmic contact (serving as the heated reservoir, red rectangle). Two current sources, S_1 and S_2, inject currents (with voltages) I_1 (V_1) and I_2 (V_2), which impinge at the floating reservoir. Equilibrating in the reservoir, they raise its temperature to T_m [9–12,25–27]. The emerging edge modes may carry net current with added thermal fluctuations, being partitioned by the QPCs; downstream QPC1@ 20µm and QPC2@ 140µm . The low frequency fluctuations (with partitioning QPCs', or not) are then measured at the *Amp* contact 240µm away.

The reservoir acquires a mean voltage, $V_m = \frac{1}{2}(I_1 + I_2)/G_H$, with $G_H = ve^2/h$ is the quantized Hall conductance at filling factor v. The dissipated power in the reservoir is $\Delta P = (I_1 - I_2)^2/4G_H$. When both currents are equal, $V_m = V_1 = V_2$, no power is dissipated in the reservoir. Using this structure, V_m and ΔP can be controlled independently with the two independent current sources [26]. A particularly interesting condition, which we exploit in this work is $I_1 = -I_2$, leading to $V_m = 0$, yet with an increased temperature of the reservoir.

The dissipated power in the floating reservoir is evacuated via two means: edge modes and lattice phonons [43–45]. Under steady state conditions the power balance equation gives,

$$\Delta P = \frac{K}{2}(T_m^2 - T_0^2) + \dot{Q}_{el-ph}(T_m, T_0) \, , \tag{1}$$

with KT_m (KT_0) the thermal conductance of edge modes at the reservoir's temperature (grounded contacts temperature). The thermal conductance of a single (ballistic) edge mode is a universal number, $\kappa_0 T = \frac{\pi^2 k_B^2}{3h}T$. Note that κ_0 is independent of the charge and the statistics of the heat carrying quasi-particles [1–4]. The term

3

$\dot{Q}_{\text{el-ph}}(T_{\text{m}}, T_0)$ represents the contribution of the lattice phonons to the dissipated heat, with an increased importance at higher temperature [43–45].

The heated small floating contact, having capacitance C, supports potential fluctuations at low frequencies with cutoff at $1/2\pi R_{\text{H}} C$ [25]; thus leading to a modified Johnson-Nyquist noise. In the limit of small capacitance $\left(2\pi R_{\text{H}} C \ll \frac{h}{k_{\text{B}} T_{\text{m}}}\right)$, the elevated reservoir's temperature is deduced by measuring the low frequency excess voltage noise at the *Amp*, $\Delta S_{\text{amp}}^{\text{V}}$, being proportional to $\Delta T = T_{\text{m}} - T_0$,

$$\Delta T = \frac{G_{\text{H}}}{k_{\text{B}}} \Delta S_{\text{amp}}^{\text{V}} . \qquad (2)$$

In Fig. 1b we present an example of the measured temperature at $v=2$, as function of I_1 and I_2 (see also Sup. Section I). Two special cases are: a diagonal white line, corresponding to $I_1 = I_2$ with $V_{\text{m}} = V_1 = V_2$ and $T_{\text{m}} = T_0$; a diagonal black line, corresponding to $I_1 = -I_2$ with $V_{\text{m}} = 0$ and $T_{\text{m}} > T_0$. In the first case partitioning of the edge modes leads to the ubiquitous shot-noise, while in the second case it leads to partitioned thermal noise (without shot noise). Our main interest here is the latter biasing conditions.

Partitioning the heated edge modes leads to added noise, which is sensitive to the energy distribution of the modes [46]. We derive a simplified model, preserving current continuity of low frequency components of the thermal noise [42] (see Sup. Section II). The partitioned thermal noise, $\Delta S^{\text{V}}(R)$, with R the reflection coefficient of the QPC and Θ a relaxation parameter,

$$\Delta S^{\text{V}}(R) = \frac{k_{\text{B}}}{G_{\text{H}}} \Delta T [R^2 + 2\Theta R(1 - R)] . \qquad (3)$$

The relaxation parameter, $\Theta = \frac{T_{\text{rel}} - T_0}{T_{\text{m}} - T_0}(1 + h)$, with h being the recently observed "thermal-shot-noise" contribution [26,47] - Θ heuristically stands (mainly) for the amount of energy dissipation. For small ΔT, $\Theta \approx \frac{T_{\text{rel}} - T_0}{T_{\text{m}} - T_0}$, and T_{rel} is an 'apparent' temperature of the edge mode at the location of the QPC.

According to Eq. 3, for a constant Θ, the partitioned thermal noise depends linearly on ΔT (Fig. 1c); corresponding data at different filling factors is shown in Fig. 2. The expected dependence of the partitioned noise on R, at different values of Θ

4

is shown in Fig. 1d, with an added data at both extremes, $\Theta = 1$ & 0, measured in $v = 2$. The red dots, measured with QPC1 partitioning, corresponds to $\Theta = 1$. The blue dots, measured with QPC2 partitioning, but after allowing the edge modes to pass through a massive floating ohmic contact at T_0, corresponds to full relaxation with $\Theta = 0$ (see Sup. Sections IV and V).

The partitioned thermal noise, by QPC1 and by QPC2, was measured as a function of ΔT, at $T_0 = 15$ mK and $R \approx 0.5$ at a few filling factors (Fig. 2). The full extent of $0 < \Theta < 1$ is shown in gray. In particle-like states, $v = 2$ and $v = 1/3$, we find $\Theta \approx 1$ at the location of QPC1, and $\Theta \approx 0.5$ at QPC2 - with the latter suggesting a significant energy dissipation. For the hole-conjugate state, $v = 2/3$, which harbors counter-propagating modes, significant dissipation is already observed in QPC1. Here, thermal equilibration is expected to take place between the counter-propagating modes [3,30,31,33]. A similar behavior is observed in $v = 1$, where edge reconstruction is known to take place, giving rise to an underlying $v = 2/3$ state [48,49]. It is worth noting that the observed linear dependence of the partitioned thermal noise in a wide range of ΔT suggests that the relaxation processes is only weakly dependent on T_m; however, as shown below, it is strongly dependent on T_0 (Fig. 3).

A further confirmation of our theoretical model was tested by measuring the normalized partitioned thermal noise $\Delta S(R)/\Delta S(R = 1)$ as a function of R at $T_0 = 15$ mK and $T_0 = 50$ mK (Fig. 3, and Sup. Section VI). The data taken at $T_0 = 15$ mK confirms the one presented in Fig. 2. However, at $T_0 = 50$ mK, severe dissipation is observed already in QPC1 in all the QHE states; being a sign of an additional relaxation process, which becomes significant at higher base temperature (such as electron-phonon coupling) [43–45]. An apparent change in the relaxation rate can be observed near $R \approx 1/2$ in the $v = 2/3$ state, which we attribute to edge reconstruction with two $v = 1/3$ edge modes and two upstream neutral modes [50–53].

While the dissipative model shown here seems to be consistent with the data, a different model was also considered (see Supp. Section III), that assumes energy equilibration among the electrons (along the propagation path) without energy loss [25]. Such equilibration model does not conserve the low frequency noise, and thus not relevant for our experiment. Alternative models [54] that conserve both total

energy and low frequency noise (not developed yet), might also be consistent with the experiment.

Here, we studied the evolution of heat propagating in QHE chiral modes. The ballistic nature of modes does not guarantee that their energy distribution remains intact a distance away. Measuring the low frequency thermal noise is not sufficient to observe the relaxation of the energy distribution, since the relaxation processes tend to preserve the low frequency components [9–12]. We employed a novel study of the evolution of the energy distribution with the propagation length. We used a structure that allowed heating a reservoir while maintaining its electro-chemical potential at zero. Two quantum point contacts, placed along the propagation path, were used to partition the heated edge modes. A simple model of the partitioned noise was found to agree with the measured data. Our findings show that energy relaxation takes place even in particle-like states (integer and fractional) as the propagation length exceeds ~100μm. Moreover, the energy relaxation length was found to strongly depend on the base temperature, suggesting that dissipation to phonons is likely to play a major role. At the same time the significant relaxation at $\nu = 2/3$, already at low temperatures and short length (~20 μm), implies that the energy exchange between the counter-propagating modes is an important mechanism of relaxation in hole-conjugate states.

References

1. J. B. Pendry, J. Phys. A Gen. Phys. **16**, 2161 (1983).

2. J. D. BEKENSTEIN and M. SCHIFFER, Int. J. Mod. Phys. C **01**, 355 (1990).

3. C. Kane and M. P. A. Fisher, Phys. Rev. B - Condens. Matter Mater. Phys. **55**, 15832 (1997).

4. L. G. C. Rego and G. Kirczenow, Phys. Rev. B - Condens. Matter Mater. Phys. **59**, 13080 (1999).

5. M. Meschke, W. Guichard, and J. P. Pekola, Nature **444**, 187 (2006).

6. K. Schwab, E. A. Henriksen, J. M. Worlock, and M. L. Roukes, Nature **404**, 974 (2000).

7. C. S. Yung, D. R. Schmidt, and A. N. Cleland, Appl. Phys. Lett. **81**, 31 (2002).

8. O. Chiatti, J. T. Nicholls, Y. Y. Proskuryakov, N. Lumpkin, I. Farrer, and D. A. Ritchie, Phys. Rev. Lett. **97**, 056601 (2006).

9. S. Jezouin, F. D. Parmentier, A. Anthore, U. Gennser, A. Cavanna, Y. Jin, and F. Pierre, Science (80-.). **342**, 601 (2013).

10. M. Banerjee, M. Heiblum, A. Rosenblatt, Y. Oreg, D. E. Feldman, A. Stern, and V. Umansky, Nature **545**, 75 (2017).

11. S. K. Srivastav, M. R. Sahu, K. Watanabe, T. Taniguchi, S. Banerjee, and A. Das, Sci. Adv. **5**, (2019).

12. M. Banerjee, M. Heiblum, V. Umansky, D. E. Feldman, Y. Oreg, and A. Stern, Nature **559**, 205 (2018).

13. A. Cappelli, M. Huerta, and G. R. Zemba, Nucl. Phys. B **636**, 568 (2002).

14. D. F. Mross, Y. Oreg, A. Stern, G. Margalit, and M. Heiblum, Phys. Rev. Lett. **121**, (2018).

15. B. Lian and J. Wang, Phys. Rev. B **97**, (2018).

16. J. Park, C. Spånslätt, Y. Gefen, and A. D. Mirlin, ArXiv:2006.06018 (2020).

17. S. H. Simon, Phys. Rev. B **97**, (2018).

18. G. Moore and N. Read, Nucl. Physics, Sect. B **360**, 362 (1991).

19. M. Levin, B. I. Halperin, and B. Rosenow, Phys. Rev. Lett. **99**, (2007).

20. S. S. Lee, S. Ryu, C. Nayak, and M. P. A. Fisher, Phys. Rev. Lett. **99**, (2007).

21. D. T. Son, Phys. Rev. X **5**, (2015).

22. C. Wang, A. Vishwanath, and B. I. Halperin, Phys. Rev. B **98**, (2018).

23. D. E. Feldman, Phys. Rev. B **98**, 167401 (2018).

24. K. K. W. Ma and D. E. Feldman, Phys. Rev. B **99**, (2019).

25. A. O. Slobodeniuk, I. P. Levkivskyi, and E. V. Sukhorukov, Phys. Rev. B - Condens. Matter Mater. Phys. **88**, 165307 (2013).

26. E. Sivre, H. Duprez, A. Anthore, A. Aassime, F. D. Parmentier, A. Cavanna, A. Ouerghi, U. Gennser, and F. Pierre, Nat. Commun. **10**, 5638 (2019).

27. E. Sivre, A. Anthore, F. D. Parmentier, A. Cavanna, U. Gennser, A. Ouerghi, Y. Jin, and F. Pierre, Nat. Phys. **14**, 145 (2018).

28. J. B. Johnson, Phys. Rev. **32**, 97 (1928).

29. H. Nyquist, Phys. Rev. **32**, 110 (1928).

30. A. Aharon-Steinberg, Y. Oreg, and A. Stern, Phys. Rev. B **99**, (2019).

31. J. Park, A. D. Mirlin, B. Rosenow, and Y. Gefen, Phys. Rev. B **99**, 161302 (2019).

32. F. Lafont, A. Rosenblatt, M. Heiblum, and V. Umansky, Science (80-.). **363**, 54 (2019).

33. C. Spånslätt, J. Park, Y. Gefen, and A. D. Mirlin, Phys. Rev. Lett. **123**, 137701 (2019).

34. H. Le Sueur, C. Altimiras, U. Gennser, A. Cavanna, D. Mailly, and F. Pierre, Phys. Rev. Lett. **105**, 34 (2010).

35. C. Altimiras, H. Le Sueur, U. Gennser, A. Cavanna, D. Mailly, and F. Pierre, Phys. Rev. Lett. **105**, 226804 (2010).

36. C. Altimiras, H. le Sueur, U. Gennser, A. Cavanna, D. Mailly, and F. Pierre, Nat. Phys. **6**, 34 (2010).

37. R. H. Rodriguez, F. D. Parmentier, D. Ferraro, P. Roulleau, U. Gennser, A. Cavanna, M. Sassetti, F. Portier, D. Mailly, and P. Roche, Nat. Commun. **1**, 2426 (2020).

38. T. Krähenmann, S. G. Fischer, M. Röösli, T. Ihn, C. Reichl, W. Wegscheider, K. Ensslin, Y. Gefen, and Y. Meir, Nat. Commun. **10**, (2019).

39. A. M. Lunde, S. E. Nigg, and M. Büttiker, Phys. Rev. B - Condens. Matter Mater. Phys. **81**, 041311 (2010).

40. P. Degiovanni, C. Grenier, G. Fève, C. Altimiras, H. Le Sueur, and F. Pierre, Phys. Rev. B - Condens. Matter Mater. Phys. **81**, (2010).

41. A. Helzel, L. V. Litvin, I. P. Levkivskyi, E. V. Sukhorukov, W. Wegscheider, and C. Strunk, Phys. Rev. B - Condens. Matter Mater. Phys. **91**, 245419 (2015).

42. C. W. J. Beenakker and M. Ḃttiker, Phys. Rev. B **46**, 1889 (1992).

43. F. C. Wellstood, C. Urbina, and J. Clarke, Phys. Rev. B **49**, 5942 (1994).

44. F. Giazotto, T. T. Heikkilä, A. Luukanen, A. M. Savin, and J. P. Pekola, Rev. Mod. Phys. **78**, 217 (2006).

45. B. Huard, H. Pothier, D. Esteve, and K. E. Nagaev, Phys. Rev. B - Condens. Matter Mater. Phys. **76**, (2007).

46. H. Inoue, A. Grivnin, N. Ofek, I. Neder, M. Heiblum, V. Umansky, and D. Mahalu, Phys. Rev. Lett. **112**, 166801 (2014).

47. O. S. Lumbroso, L. Simine, A. Nitzan, D. Segal, and O. Tal, Nature **562**, 240 (2018).

48. V. Venkatachalam, S. Hart, L. Pfeiffer, K. West, and A. Yacoby, Nat. Phys. **8**, 676 (2012).

49. R. Bhattacharyya, M. Banerjee, M. Heiblum, D. Mahalu, and V. Umansky, Phys. Rev. Lett. **122**, 246801 (2019).

50. R. Sabo, I. Gurman, A. Rosenblatt, F. Lafont, D. Banitt, J. Park, M. Heiblum, Y. Gefen, V. Umansky, and D. Mahalu, Nat. Phys. **13**, 491 (2017).

51. A. Rosenblatt, F. Lafont, I. Levkivskyi, R. Sabo, I. Gurman, D. Banitt, M. Heiblum, and V. Umansky, Nat. Commun. **8**, 2251 (2017).

52. Y. Meir, Phys. Rev. Lett. **72**, 2624 (1994).

53. J. Wang, Y. Meir, and Y. Gefen, Phys. Rev. Lett. **111**, 246803 (2013).

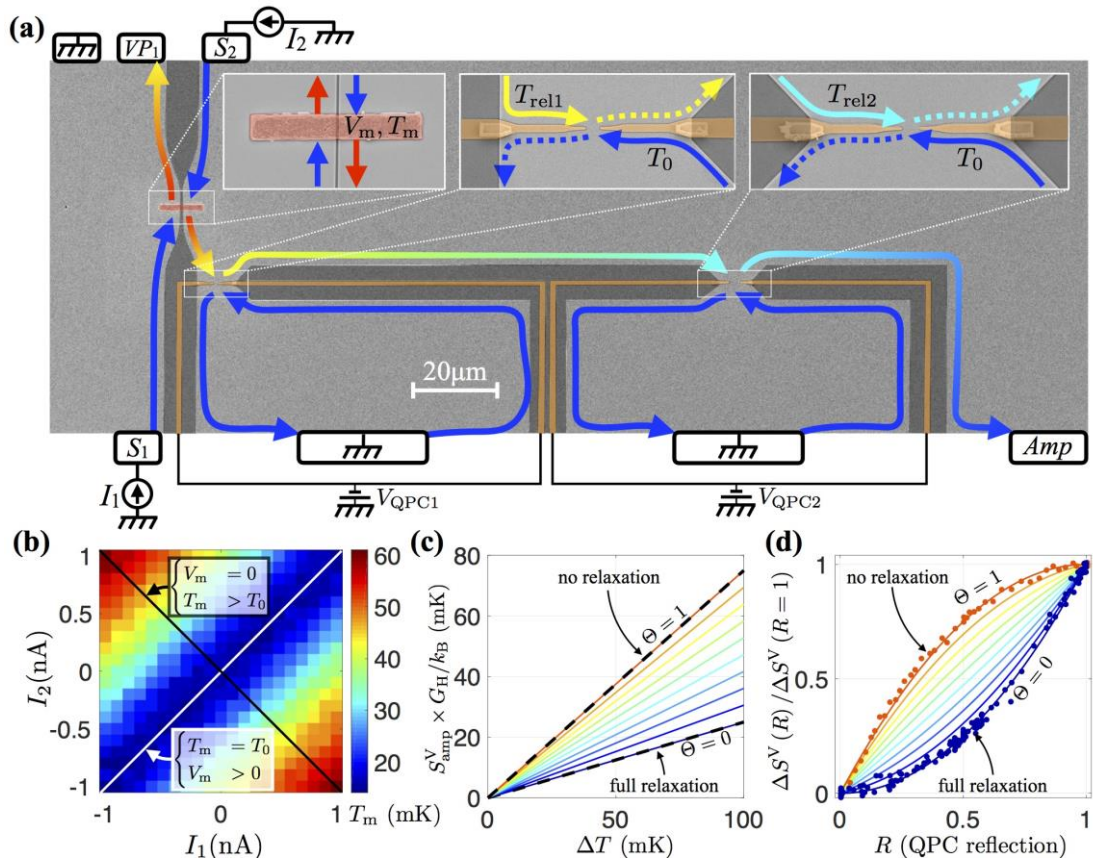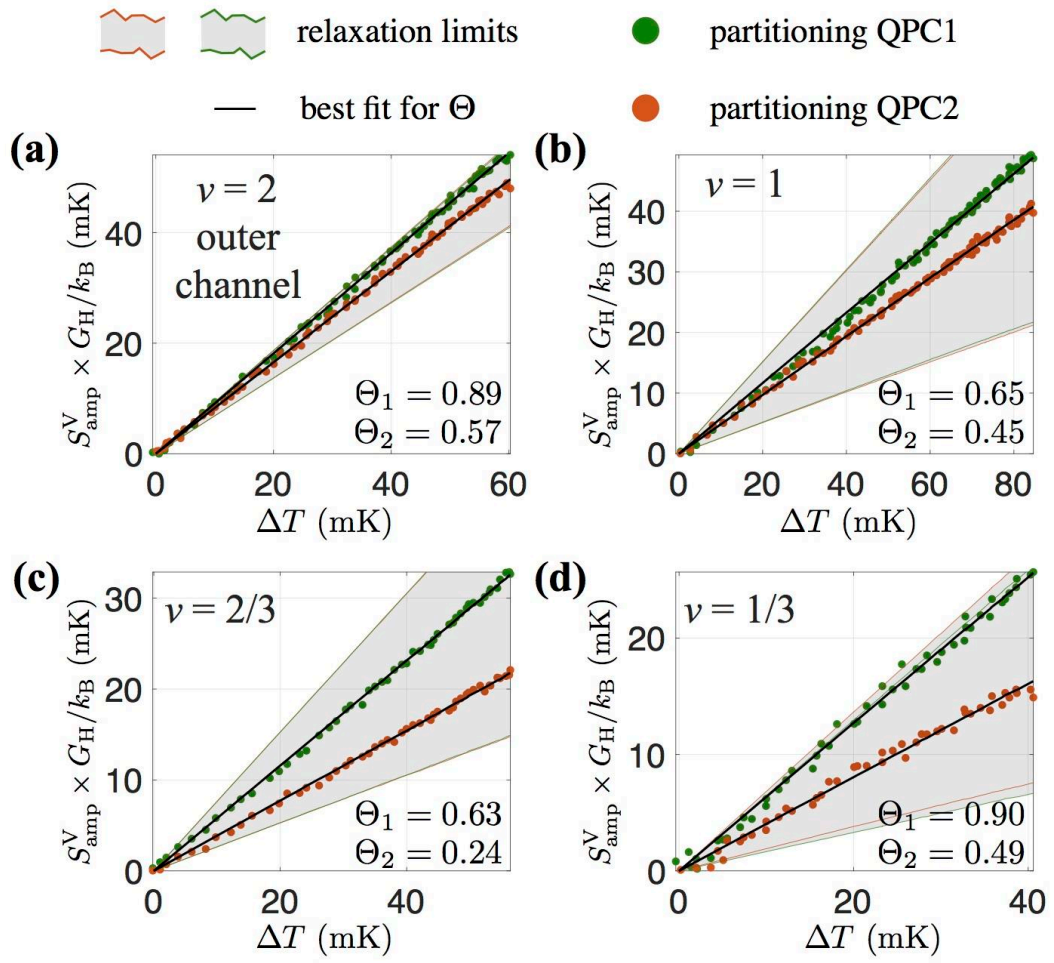54. M. Rigol, V. Dunjko, V. Yurovsky, and M. Olshanii, Phys. Rev. Lett. **98**, 050405 (2007).
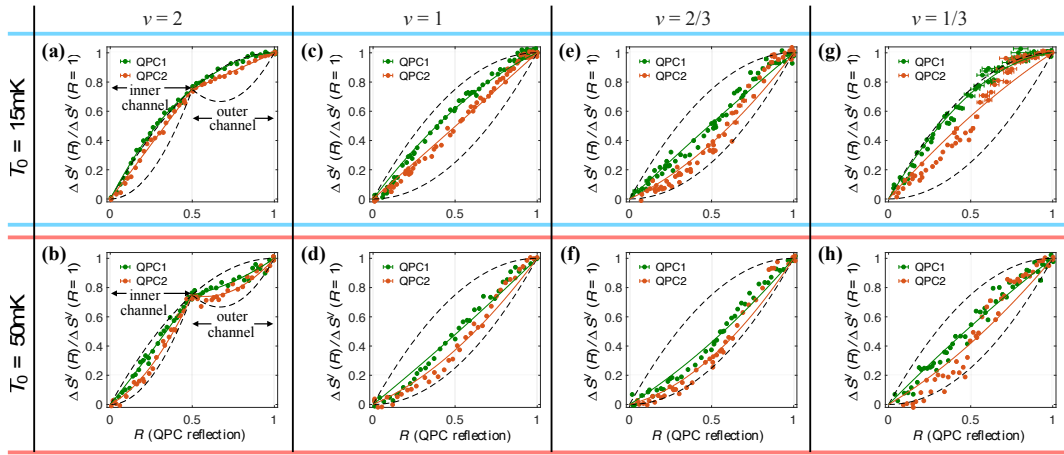
Figure 1

Figure 2

Figure 3

Figure captions

Figure 1. (a) Scanning electron microscope image of the device: two mesas, separated by an etched groove (dark grey), are connected by a small floating ohmic contact ($10 \times 1.5 \mu m^2$). Two QPCs defined by gates (brown) are placed downstream at 20μm and 140μm away from the floating contact. Two DC sources, S_1 and S_2, with voltages V_1 and V_2, and currents I_1 and I_2 charge the floating ohmic contact, and heat it up. An amplifier, placed 240μm downstream away from the contact, measures the voltage noise. **(b)** Measured temperature of the floating contact, T_m, as function of I_1 and I_2, at $v = 2$ and $T_0 = 15mk$. The temperature is extracted from the measured Johnson-Niquist noise, when both QPCs are fully pinched. **(c)** Theoretical partitioned thermal-noise at one of the QPCs as function of $\Delta T = T_m - T_0$. when $V_m = 0$, at a constant reflection coeficient, $R = 1/2$. **(d)** Normalized partitioned thermal noise as function of the reflection coefficient of the QPC, R, for different values of the relaxation parameter Θ at a constant ΔT. Red dots: Data measured with partitioning by QPC1 at $v = 2$. Blue dots: Data measured with partitioning by QPC2 at $v = 2$ after cooling down the edge modes.

Figure 2. Partitioned thermal noise as function of temperature difference ΔT at a constant reflection coefficient $R \approx 1/2$, at $T_0 = 15mK$. Green circles – partitioning by QPC1 while keeping QPC2 fully pinched, Orange circles- partitioning by QPC2 while keeping QPC1 fully pinched. Grey region – limits of the theoretical model. Lower limit corresponds to full relaxation, $\Theta = 0$ and upper limit corrsponds to $\Theta = 1$. Black lines – linear fit for the relaxation parameter, Θ, using Eq. 3. **(a)** $v = 2$ outer channel, **(b)** $v = 1$, **(c)** $v = 2/3$, **(d)** $v = 1/3$.

Figure 3. Partitioned thermal noise as a function of the reflection coeficient at a constant temperature difference. Green circles – partitioning QPC1 while keeping QPC2 fully pinched; Orange circles - partitioning QPC2 while keeping QPC1 fully pinched; Dashed black lines – limits of the theoretical model, lower limit corresponds to full relaxation $\Theta = 0$ and upper limit corrsponds to $\Theta = 1$. Best fit of the relaxation parameter, Θ_1 for QPC1 (green solid line) and Θ_2 for QPC2 (orange solid line), using Eq. 3. **(a)** $\Theta_{1inner} = 1.07, \Theta_{1outer} = 0.97$; $\Theta_{2inner} = 0.75, \Theta_{2outer} = 0.75$. **(b)** $\Theta_{1inner} = 0.7, \Theta_{1outer} = 0.6$; $\Theta_{2inner} = 0.31, \Theta_{2outer} = 0.3$. **(c)** $\Theta_1 = 0.74$, $\Theta_2 = 0.49$. **(d)** $\Theta_1 = 0.46$, $\Theta_2 = 0.24$. **(e)** $\Theta_1 = 0.53$, $\Theta_2 = 0.26$. **(f)** $\Theta_1 = 0.35, \Theta_2 = 0.15$. **(g)** $\Theta_1 = 0.94, \Theta_2 = 0.63$. **(h)** $\Theta_1 = 0.57, \Theta_2 = 0.34$.

Supplementary Materials

Energy relaxation in edge modes in the quantum Hall effect

Amir Rosenblatt[1], Sofia Konyzheva[1], Fabien Lafont[1], Noam Schiller[1], Jinhong Park[2], Kyrylo Snizhko[1], Moty Heiblum[1], Yuval Oreg[1] and Vladimir Umansky[1]

1. *Braun Center for Submicron Research, Department of Condensed Matter Physics, Weizmann Institute of Science, Rehovot 761001, Israel*

2. *Institute for Theoretical Physics, University of Cologne, Zülpicher Str. 77, 50937 Köln, Germany*

I.   Measuring T_m and the quantum limit of heat flow

With the two QPCs are fully pinched, the voltage noise was measured at the amplifier's contact as function of the injected currents, $I_1 = -I_2$, keeping $V_m = 0$. In Fig. S1a, we plot the temperature T_m, rendered from the measured noise, exploiting Eq. 2. In Fig. S1b we plot T_m as a function of the dissipated power ΔP in all the filling factors. The quantum limit of heat is determined from the expression of the power balance:

$$\Delta \mathrm{P} = \frac{K}{2}(T_m^2 - T_0^2) + \beta_{\text{el-ph}}(T_m^5 - T_0^5)\,, \tag{S1}$$

with KT_m (KT_0) the thermal conductance of edge modes leaving the reservoir (leaving grounded contacts). The thermal conductance of a single (ballistic) edge mode is a universal number, $KT = \kappa_0 T = \frac{\pi^2 k_B^2}{3h}T$. The heat carried by the phonons is expected to have a T^5 dependence, and $\beta_{\text{el-ph}}$ is the electron-phonon coupling constant, which depends on the volume of the heated reservoir [1–3]. The heat power measurements for $\nu = 3,\ 2$ and 1 (Fig. S1b, circles) agrees with the quantum heat power with $6\kappa_0, 4\kappa_0$ and $2\kappa_0$, for the two-arm device, respectively (Fig. S1b, black curves) with $\beta_{\text{el-ph}} = 7$ nW/K^5. Heat power measurements for the fractional $\nu = 1/3$, agrees with $2\kappa_0$ as expected. At the hole-conjugate state $\nu = 2/3$, one should expect zero heat conductance at long distance, due to energy transfer between

1

counter-propagating edge modes. These results, reproduce the quantum limited heat flow measured before [4–6].

II.   Theoretical model: dissipation

Our model attempts to describe the experimental results for integer quantum Hall states with minimal physical assumptions. Current continuity at low frequencies is assumed; namely, no charge accumulates anywhere along the edge [7]. A fictitious floating contact, placed right before the QPC models the dissipation (Fig. S2). From here, we follow standard methods of calculating zero-frequency fluctuations in mesoscopic circuits [8–10].

The fictitious floating contact is assumed to have temperature T_{rel}, corresponding to the effective (cooled) temperature of the mode at the point of partitioning. Hence, this temperature spans the range $T_0 \leq T_{\text{rel}} \leq T_{\text{m}}$, with the lower and upper bounds representing full and no relaxation, respectively. No explicit assumptions are made as to the mechanism leading to relaxation, but as noted in the main text, the prominence of relaxation at higher base temperatures points at electron-phonon interactions as a reasonable culprit.

We begin with the integer state $\nu = 1$; generalization to higher filling factors is straightforward. The currents at our real, small floating contact, I_{m}; at the fictitious floating contact, I_{C}; and at the amplifier, I_{Amp}, are given by the equations

$$I_{\text{m}} = G_1(V_{\text{m}} - V_1) + G_2(V_{\text{m}} - V_2) + \delta I_{\text{m}} \ , \qquad (S2a)$$

$$I_{\text{C}} = G_1(V_{\text{C}} - V_{\text{m}}) + \delta I_{\text{C}} \ , \qquad (S2b)$$

$$I_{\text{Amp}} = G_1\left(V_{\text{Amp}} - RV_{\text{C}}\right) + \delta I_{\text{Amp}} \ . \qquad (S2c)$$

Here, G_i is the conductance in the ith side of the mesa (we will later take $G_1 = G_2 = G_{\text{H}}$), R is the QPC's reflection coefficient, and δI_j describes uncorrelated current fluctuations leaving contact j. Subtracting the average value of these three currents, we find,

$$\Delta I_{\text{m}} = (G_1 + G_2)\delta V_{\text{m}} + \delta I_{\text{m}} \ , \qquad (S3a)$$

$$\Delta I_{\text{C}} = G_1(\delta V_{\text{C}} - \delta V_{\text{m}}) + \delta I_{\text{C}} \ , \qquad (S3b)$$

$$\Delta I_{\text{Amp}} = -G_1 R \delta V_{\text{C}} + \delta I_{\text{Amp}} \ , \qquad (S3c)$$

where $\Delta I_j \equiv I_j - \langle I_j \rangle$ and $\delta V_j \equiv V_j - \langle V_j \rangle$. We emphasize that only the floating contacts have non-zero voltage fluctuations, since all other reservoirs are kept at constant chemical potential. Hence, only δV_m, $\delta V_\mathrm{C} \neq 0$. The value of the voltage fluctuations is determined by our assumption that no charge accumulates at the floating contacts, i.e. $\Delta I_\mathrm{m} = \Delta I_\mathrm{C} = 0$ [7]. Thus, Eq. S3 directly gives,

$$\Delta I_\mathrm{Amp} = R \frac{G_1}{G_1 + G_2} \delta I_\mathrm{m} + R \delta I_\mathrm{C} + \delta I_\mathrm{Amp} . \tag{S4}$$

The voltage noise fluctuations measured at the amplifier are defined via the correlation function, $S^\mathrm{V} \equiv \frac{1}{G_1^2} \langle \Delta I_\mathrm{Amp} \Delta I_\mathrm{Amp} \rangle$,

$$G_1^2 S^\mathrm{V} = R^2 \left[\left(\frac{G_1}{G_1 + G_2} \right)^2 S_\mathrm{m,m}^\mathrm{eq} + 2 \frac{G_1}{G_1 + G_2} S_\mathrm{m,C}^\mathrm{eq} + S_\mathrm{C,C}^\mathrm{eq} \right]$$
$$+ 2R \left[\frac{G_1}{G_1 + G_2} S_\mathrm{m,Amp}^\mathrm{eq} + S_\mathrm{C,Amp}^\mathrm{eq} \right] + S_\mathrm{Amp,Amp}^\mathrm{eq} , \tag{S5}$$

where we define $S_{i,j}^\mathrm{eq} \equiv \langle \delta I_i \delta I_j \rangle$, using the zero-frequency limit of the canonical formula for noise correlations [10,11],

$$S_{ij}^\mathrm{eq}(\omega) = \frac{e^2}{h} \sum_{k,l} \sum_{m,n} \int dE \, A_{kl}^{mn}(i; E, E + \hbar\omega) A_{lk}^{nm}(j; E + \hbar\omega, E)$$
$$\times \{ f_k(E)[1 - f_l(E + \hbar\omega)] + f_l(E + \hbar\omega)[1 - f_k(E)] \} . \tag{S6}$$

Here, k, l are summed over terminals. m, n are summed over channel numbers with values between 1 and the filling factor (and are hence trivial for filling factor 1). $f_k(E) = \frac{1}{e^{\frac{E - \mu_k}{k_\mathrm{B} T_k}} + 1}$ is the Fermi-Dirac distribution of the electrons that exit contact k. A is determined by the scattering matrix of the problem via,

$$A_{kl}^{mn}(i; E, E') = \delta_{ik} \delta_{il} \delta_{mn} - \sum_p s_{ik;mp}^\dagger(E) s_{il;pn}(E') , \tag{S7}$$

where $s_{ik;mn}(E)$ denotes the scattering probability of an electron at energy E, from channel m in contact i, to channel n in contact k. Performing explicit calculations with all terms of this form in Eq. S5, we obtain,

$$S^\mathrm{V} = 2 \frac{k_\mathrm{B}}{G_1} \left[\frac{G_2}{G_1 + G_2} R^2 (T_\mathrm{m} - T_0) + R(1 - R)(T_\mathrm{rel} - T_0) \left(1 + h\left(\frac{T_\mathrm{rel}}{T_0} \right) \right) + 2T_0 \right] , \tag{S8}$$

where $h\left(\frac{T_\mathrm{rel}}{T_0} \right)$ is the thermal-shot-noise obtained from partitioning channels with different temperatures [12,13], given by the expression

$$h\left(\frac{T_{\text{rel}}}{T_0}\right) = \frac{1}{k_B(T_{\text{rel}} - T_0)} \int dE \left(\frac{1}{e^{\frac{E}{T_{\text{rel}}}} + 1} - \frac{1}{e^{\frac{E}{T_0}} + 1}\right)^2. \qquad (S9)$$

It is worth noting at this stage that for $R = 0, 1$, the effective local temperature T_{rel} drops entirely out of the expression, consistent with the expectation that temperature changes along the edge do not affect low-frequency noise in the absence of partitioning.

Focusing exclusively on the excess noise, $\Delta S^V = S^V - S^V(T_m = T_0)$, with $G_1 = G_2 = G_H$, and $\Theta \equiv \frac{T_{\text{rel}} - T_0}{T_m - T_0}\left(1 + h\left(\frac{T_{\text{rel}}}{T_0}\right)\right)$, the excess noise reduces to the rather compact expression used in Eq. 3,

$$\Delta S^V = \frac{k_B}{G_H}[R^2 + 2\Theta R^2(1 - R^2)](T_m - T_0). \qquad (S10)$$

It is worth dwelling on the nature of this thermal shot noise. The asymptotic values of $h\left(\frac{T_{\text{rel}}}{T_0}\right)$, as described in Eq. S9, are: $\lim_{T_{\text{rel}} \to T_0} h\left(\frac{T_{\text{rel}}}{T_0}\right) \propto (T_{\text{rel}} - T_0)$, and $\lim_{\frac{T_{\text{rel}}}{T_0} \to \infty} h\left(\frac{T_{\text{rel}}}{T_0}\right) \approx 0.38$. This means that for a small ΔP this h term can entirely be neglected; yet, even at high T_m, its contribution does not dominate the measured noise.

The constraint $T_{\text{rel}} \leq T_m$ dictates $\Theta \leq 1 + h\left(\frac{T_m}{T_0}\right)$, with a maximum of $\Theta \approx 1.38$. In particular, the thermal shot noise contribution explicitly leads to $\Theta > 1$ for no relaxation. We did not find values of Θ that are larger than unity, hinting that all measured configurations exhibit some relaxation.

Generalization of the result in Eq. S10 to integer filling factors other than 1 is rather straightforward. For an integer filling factor v, we have in total v edge channels, and we assume that each channel $1 \leq n \leq v$ is described by its own effective temperature $T_{\text{rel},n}$ and its own reflection coefficient $0 < R_n < 1$, with the total reflection coefficient of the QPC determined by $R = \frac{1}{v}\sum_{n=1}^{v} R_n$. Carefully repeating the above steps, we arrive at the general formula,

$$\Delta S_v^V = 2\frac{k_B v}{G_H}\left[\sum_{n=1}^{v}\left(1 - \frac{1}{2v}\right)R_n^2 - \frac{1}{v}\sum_{n'>n=1}^{v} R_n R_{n'} + \sum_{n=1}^{v}\Theta_n R_n (1 - R_n)\right]$$
$$\times (T_m - T_0), \qquad (S11)$$

where once again, $\Theta_n \equiv \frac{T_{\text{rel,n}} - T_0}{T_m - T_0}\left(1 + h\left(\frac{T_{\text{rel,n}}}{T_0}\right)\right)$.

It is important to note that mode-dependent quantities are not mutually independent. Since the QPC partitions channels from the inside to outside, at any given point there is only one channel that is not fully reflected or fully transmitted. Thus, for any given value of $R = \frac{1}{\nu}\sum_{n=1}^{\nu} R_n$, all values of R_n are well defined. Additionally, as argued above and readily apparent from Eq. S11, the measured noise is independent of all effective temperatures $T_{\text{rel},i}$ of the modes that are fully reflected or transmitted. Thus, the only free parameter in Eq. S11 is $T_{\text{rel},j}$ for the single partitioned channel j. In particular, at $R = \frac{q}{\nu}$ at filling factor ν, which corresponds to q fully transmitted channels and $-q$ fully reflected channels, we obtain,

$$\frac{\Delta S^V\left(R = \frac{q}{\nu}\right)}{\Delta S^V(R = 1)} = \left(\frac{q}{\nu}\right)^2 + 2\left(\frac{q}{\nu}\right)\frac{\nu - q}{\nu}. \tag{S12}$$

These specific values fit our data very well for $\nu = 2, 3$ (see Fig. 3 and Fig. S5), thus providing strong support for our model.

III.   Theoretical model – equilibration

In parallel to the model described in the previous section, further efforts were made to model energy relaxation through redistribution of energies without loss. Our assumption was that this redistribution eventually arrives at the thermodynamic limit of an equilibrium Fermi-Dirac distribution. Such a distribution at temperature T and no bias voltage corresponds to a frequency-dependent noise correlation function of

$$S_T(\omega) = G_H \hbar\omega \coth\left(\frac{\hbar\omega}{2k_B T}\right), \tag{S13}$$

giving zero-frequency noise of $S_T(\omega = 0) = 2k_B G_H T$, and a total energy of $\int d\omega S_T\, \omega \propto (k_B T)^2$. As such, both the zero-frequency noise and total energy are mutually determined by a single parameter, and cannot be separately tuned to any pair of desired values. Consequently, by assuming an energy conserving Fermi-Dirac equilibrium, we explicitly broke zero-frequency noise conservation.

This assumption was ultimately not borne out in the data. As such, a model assuming equilibration along the edge towards a Fermi-Dirac distribution, along the lines of Ref. [14], was insufficient in explaining our measurements. In particular, such a model fails to recreate the results of Eq. S12, which serve as a stark feature of the

measurement and are obtained through the zero-frequency conservation assumed in Supp. Section II.

IV. Measurement methodology of partitioned thermal noise

This section demonstrates the methodology of how to determine the thermal relaxation. Using the device presented in Fig. S1a, DC power ΔP is applied while $V_{\mathrm{m}} = 0$, in order to heat the small floating contact but keep its potential at zero. The hot edge modes leaving the small floating contact, encounter two QPCs: QPC1 at distance 20μm away from the small floating contact and QPC2 at 140μm away. On each QPC we can partition the hot edge - flowing on one side, with the grounded edge at T_0 - flowing on the other side, resulting partitioned thermal noise, free of any shot-noise.

First, the reflected differential conductance of each QPC is measured with small AC voltage $\sim 0.5 \ \mu V_{\mathrm{RMS}}$ such that it has negligible heating. The measurement was done both with and without DC heating and will denote it as an error in the coming plots. We note that the reflected differential conductance of either QPCs has almost no dependence on the heating. The reflected differential conductance of each QPC is measured while scanning the QPC gate voltage, as the other QPC was fully pinched (Fig. S3a). Next, we applied constant DC heating power ΔP raising its temperature to some T_{m}, while keeping $V_{\mathrm{m}} = 0$. The partitioned thermal noise was measured at the amplifier as function of the split-gate voltage V_{QPC} of each QPC (Fig. S3b).

In order to determine the thermal relaxation, we plot the normalized partitioned thermal noise as function of the reflection coefficient R, in Fig. S3c. The upper black curve indicates the non-relaxed limit ($\Theta = 1$), the lower black curve indicates the fully relaxed limit ($\Theta = 0$, for a single edge mode) and the dashed black curves indicate the fully relaxed limit for two edge modes ($\Theta = 0$, for each edge mode).

V. Testing the full relaxation limit

In this section we probe the partitioned thermal noise of a fully relaxed edge mode. The edge mode is cooled down by entering into a massive floating contact, strongly

coupled to the lattice temperature T_0 with electron-phonon interactions. The electron-phonon interaction is proportional to the volume of the contact. The massive ohmic contact volume is $10 \times 60 \times 0.2 \mu m^3$, which is ~40 times bigger than the small floating contact. In addition, it is connected to a large metallic pad ($80 \times 80 \mu m^2$), also contributing to thermalization. The RC cutoff frequency of such thermalizing contact is estimated to be in the $\sim 100\text{MHz}$ range, which is much smaller than the temperature cutoff ($\sim$ GHz range) and much larger than the measuring frequency $\sim$ 1 MHz.

The partitioned thermal noise was measured at $\nu = 2$ in two cases: (1) partitioning at QPC1, keeping QPC2 fully pinched (Fig. S4a); (2) keeping QPC1 open, allowing the channel to pass through the massive floating contact and partitioning at QPC2 (Fig. S4c). In case (1), the partitioned thermal noise (Fig. S4b), corresponds to non-relaxed edge modes. In case (2), the partitioned thermal noise corresponds to a fully relaxed single edge mode (Fig. S4d), as expected by the equilibration of the two edge modes inside the massive floating contact.

Note that the same amount of low frequency noise was measured when QPC2 is fully pinched, without any difference whether QPC1 is open or close, confirming conservation of low frequency current on the massive floating contact.

VI.   Thermal relaxation of edge modes vs. reflection coefficient

Following the measurement procedure presented in Sup. section IV, a constant DC heating ΔP applied while keeping $V_m = 0$, raising the small floating contact's temperature to some T_m. The partitioned thermal noise is measured as function of the reflection coefficient of the QPC. The normalized noise $\Delta S(R)/\Delta S(R = 1)$ is presented in Fig. S5 for particle-like states ($\nu = 3, 2, 1/3$) and in Fig. S6 for hole-conjugate states ($\nu = 1 +$ at 3.2 T, the low field side of the $\nu = 1$ plateau; $\nu = 1 -$ at 3.75 T, the high field side of the $\nu = 1$ plateau; and $\nu = 2/3$) together with a fit of the dimensionless relaxation parameter Θ for each edge mode, such that:

$$\frac{\Delta S^V(R)}{\Delta S^V(R = 1)} = \quad R^2 + 2\Theta R(1 - R), \qquad\qquad (S14)$$

where $0 < \Theta < 1 + h\left(\frac{T_m}{T_0}\right)$. The limit $\Theta = 0$ corresponds to full relaxation (lower black dashed curve); the limit $\Theta = 1 + h\left(\frac{T_m}{T_0}\right)$ corresponds to no relaxation (upper black dashed curve); and the limit $\Theta = 1$ corresponds to no relaxation with zero thermal-shot-noise contribution $h = 0$ (upper black solid curve). A model for multichannel case (such as in $v = 2$ and 3) is found in Sup. section II. Noise measured with partitioning QPC1, placed 20μm away from the small floating contact, plotted in green circles. Noise measured with partitioning QPC2, placed 140 μm away from the small floating contact, plotted in orange circles.

Filling factor $v = 1$ is known to experience edge reconstruction, giving rise to an underlying $v = 2/3$ state [15,16]. This is also suggested from our measurements, having pronounce relaxation at $v = 1$ (Fig. S6), growing stronger at the high field side of the $v = 1$ plateau, where the reconstruction is expected to appear [15].

VII. Device fabrication

The GaAs/AlGaAs heterostructure used in the report (#C2-287), has electron density $n = 0.90 \times 10^{11} \text{cm}^{-2}$ and dark mobility $\mu = 4.6 \times 10^6 \text{cm}^2\text{V}^{-1}\text{s}^{-1}$ measured at 4.2K, with the 2DEG buried 1280Å below the surface. For the ohmic contacts, evaporation of the sequence: Ni 50 Å, Au 1900 Å, Ge 1000 Å, Ni 710 Å, Au 150 Å, followed by annealing at 120°C for 120 sec, followed by 360°C for 30 sec, and 440°C for 50 sec. For all the metallic gates on the device, such as QPCs, we evaporated of Ti 50 Å followed by Au 150Å, employing lift-off techniques.

VIII. Calibration of the amplifier

We calibrated the amplifier using two methods: the first using shot-noise at $v = 2$ (Fig. S7a). The outer channel was partitioned and the noise was measured as function of the current (injecting two currents with the same polarity, $I_1 = I_2$), leaving the small floating ohmic contact at a finite voltage and zero power dissipation. We used the ubiquitous shot-noise equation [11]:

$$\Delta S^{\text{I}} = 2eIR(1 - R)\left[\coth(x) - \frac{1}{x}\right], \#(S15)$$

where $x = \frac{eI}{2k_{\mathrm{B}}TG_{\mathrm{H}}}$. Gain and electron temperature were fitted with Gain = 8.8 and $T = 15$ mK. Another calibration method used the Johnson-Nyquist noise [17,18], $S^{\mathrm{I}} = \text{Gain} \times 4k_{\mathrm{B}}TG_{\mathrm{H}}$, at a few fridge base temperature, ranging from $T = 15$ mK to $T = 300$mK, where $G_{\mathrm{H}} = 2e^2/h$ at $\nu = 2$ (Fig. S7b). The fitted Gain=8.9 ± 0.2 - in agreement with the previous shot-noise fit. The intercept of the linear fit with $T = 0$ gives the characteristic noise of the amplifier, 270 pV/√Hz.

References

1. F. C. Wellstood, C. Urbina, and J. Clarke, Phys. Rev. B **49**, 5942 (1994).

2. B. Huard, H. Pothier, D. Esteve, and K. E. Nagaev, Phys. Rev. B - Condens. Matter Mater. Phys. **76**, (2007).

3. F. Giazotto, T. T. Heikkilä, A. Luukanen, A. M. Savin, and J. P. Pekola, Rev. Mod. Phys. **78**, 217 (2006).

4. S. Jezouin, F. D. Parmentier, A. Anthore, U. Gennser, A. Cavanna, Y. Jin, and F. Pierre, Science (80-.). **342**, 601 (2013).

5. M. Banerjee, M. Heiblum, A. Rosenblatt, Y. Oreg, D. E. Feldman, A. Stern, and V. Umansky, Nature **545**, 75 (2017).

6. S. K. Srivastav, M. R. Sahu, K. Watanabe, T. Taniguchi, S. Banerjee, and A. Das, Sci. Adv. **5**, (2019).

7. C. W. J. Beenakker and M. Bttiker, Phys. Rev. B **46**, 1889 (1992).

8. M. Büttiker, Phys. Rev. B **46**, 12485 (1992).

9. U. Sivan and Y. Imry, Phys. Rev. B **33**, 551 (1986).

10. M. Anantram and S. Datta, Phys. Rev. B - Condens. Matter Mater. Phys. **53**, 16390 (1996).

11. Y. M. Blanter and M. Büttiker, Phys. Rep. **336**, 1 (2000).

12. E. Sivre, H. Duprez, A. Anthore, A. Aassime, F. D. Parmentier, A. Cavanna, A. Ouerghi, U. Gennser, and F. Pierre, Nat. Commun. **10**, 5638 (2019).

13. O. S. Lumbroso, L. Simine, A. Nitzan, D. Segal, and O. Tal, Nature **562**, 240 (2018).

14. A. O. Slobodeniuk, I. P. Levkivskyi, and E. V. Sukhorukov, Phys. Rev. B - Condens. Matter Mater. Phys. **88**, 165307 (2013).

15. V. Venkatachalam, S. Hart, L. Pfeiffer, K. West, and A. Yacoby, Nat. Phys. **8**, 676 (2012).

16. R. Bhattacharyya, M. Banerjee, M. Heiblum, D. Mahalu, and V. Umansky, Phys. Rev. Lett. **122**, 246801 (2019).

17. J. B. Johnson, Phys. Rev. **32**, 97 (1928).

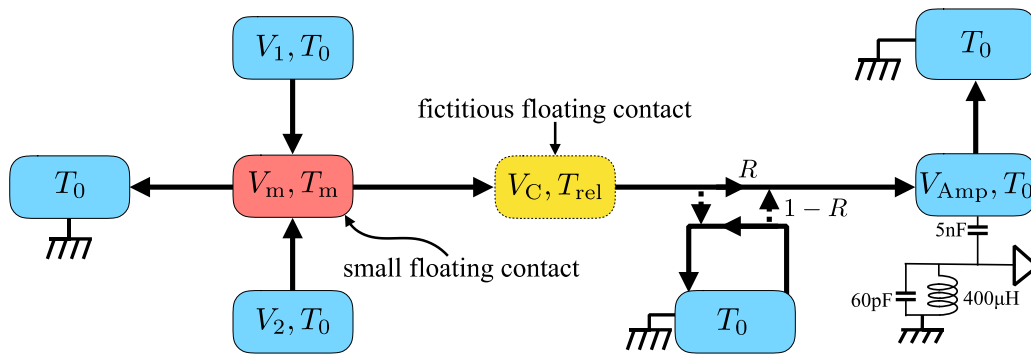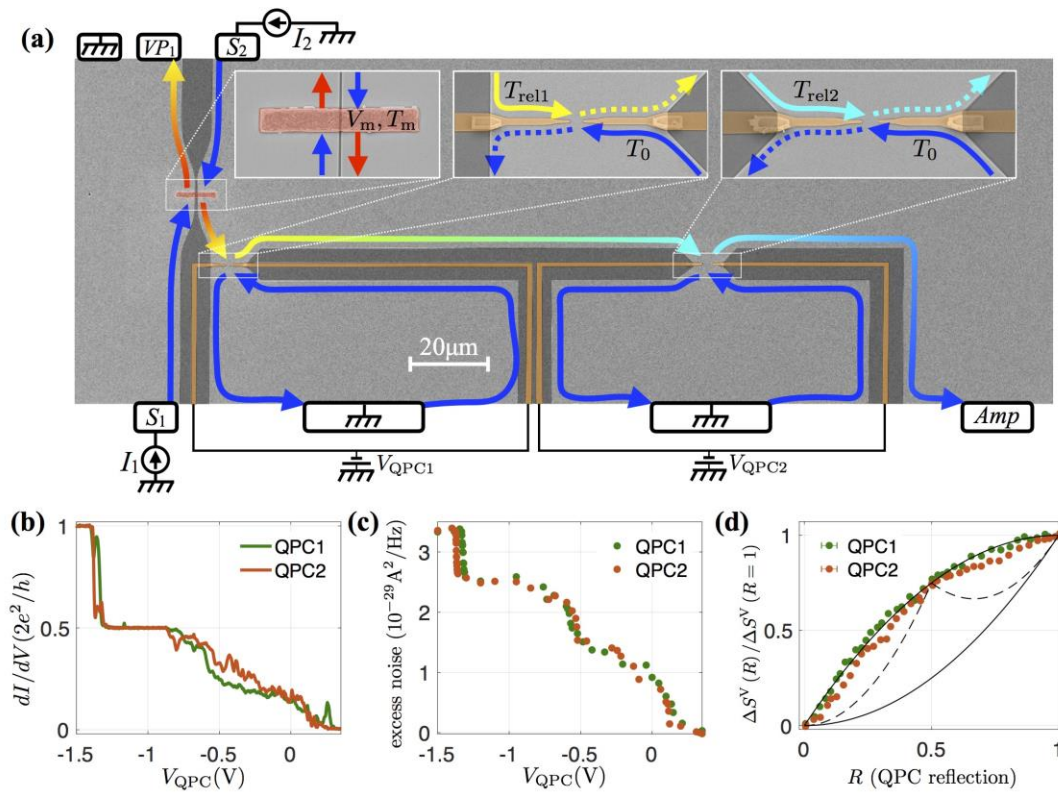18. H. Nyquist, Phys. Rev. **32**, 110 (1928).

Supplementary Figures

(a)

(b)
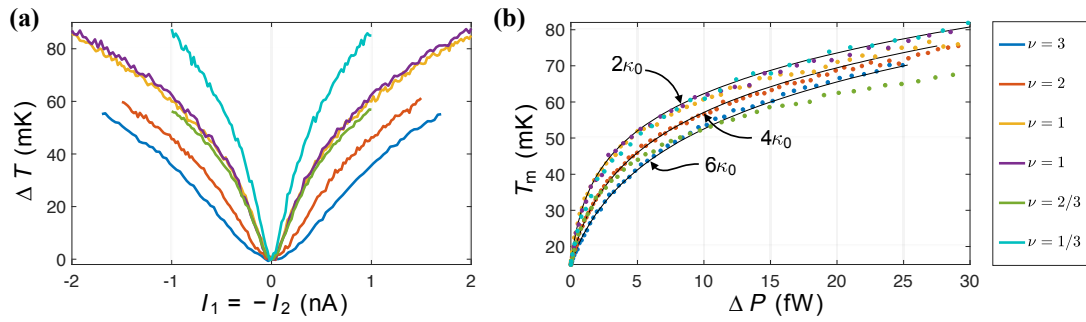
Figure S1

Figure S2

11
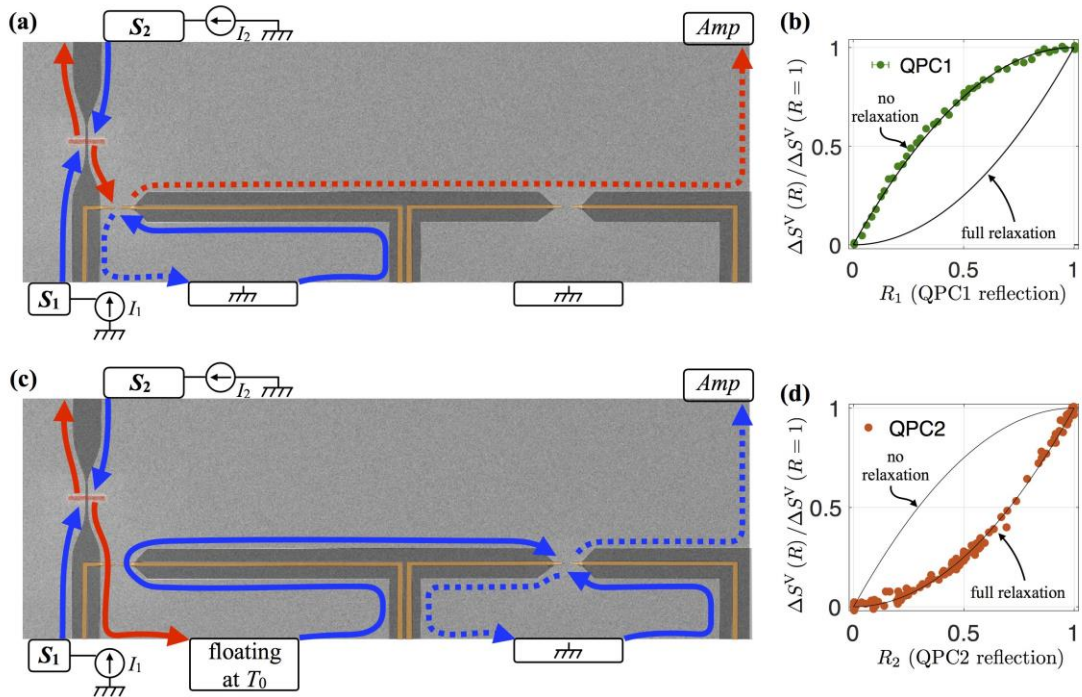
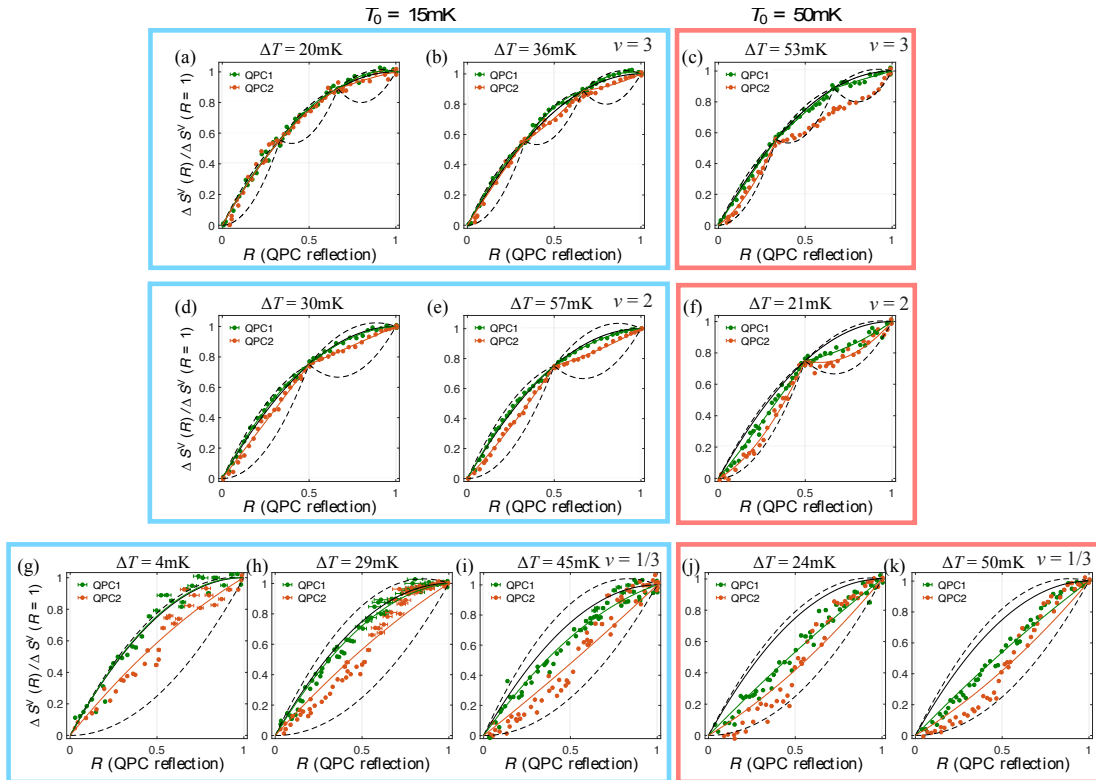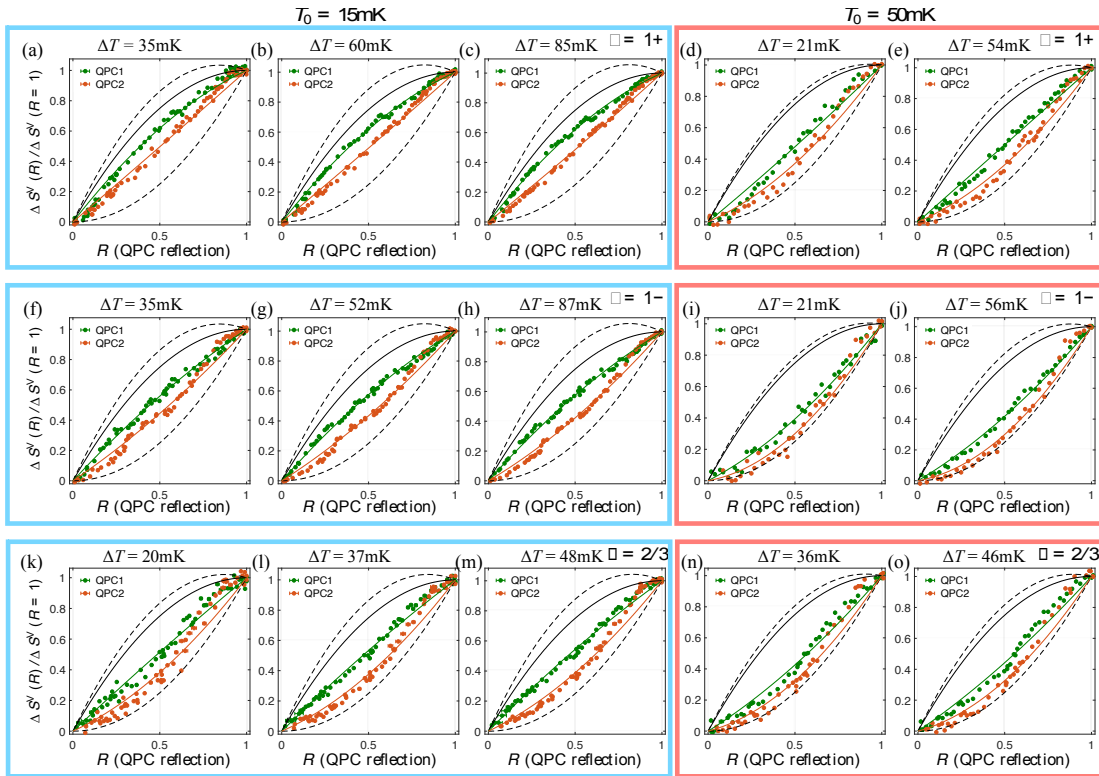**Figure S3**
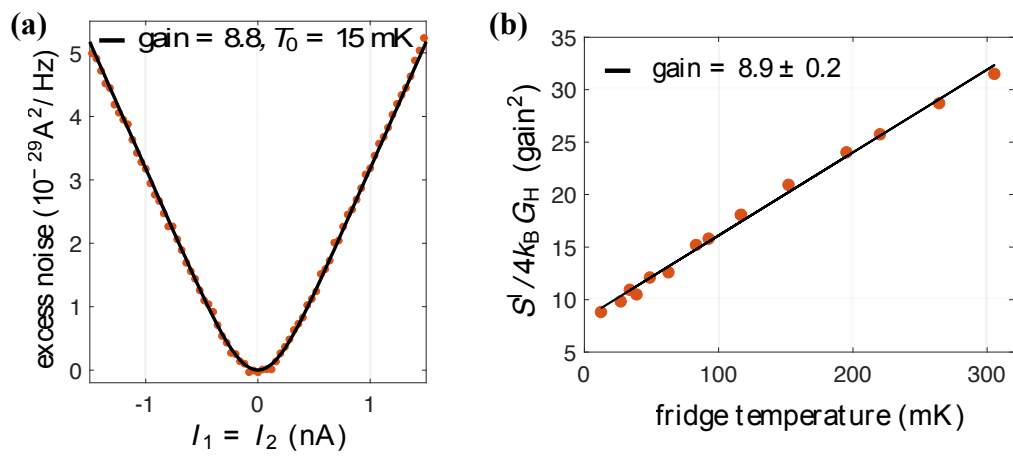

Figure S4

Figure S5

Figure S6

Figure S7

Supplementary Figures Captions

Figure S1. **Temperature calibration of the small floating contact and the quantum limit of heat flow.** (a) Measurement of small floating contact's temperature T_m as function of the heating current $I_1 = -I_2$, at base temperature $T_0 = 15$ mK . Measured when both QPCs are fully closed, at filling factors v =3,2,1,2/3 and 1/3 , where at v =1 we measure on the low field side of the plateau (yellow) and on the high filed side (purple). (b) Temperature as function of the dissipated power ΔP for all measured filling factors, dashed black curves represents the theoretical quantum limit of heat flow for 2, 4 and 6 modes with electron-phonon term $\dot{Q}_{el-ph} = \beta_{el-ph}(T_m^5 - T_0^5)$ where $\beta_{el-ph} = 7$nW/K^5 .

Figure S2. **Schematic description of the dissipation model**. Current flows from two sources at voltages V_1, V_2 and temperature T_0 to a floating contact. The floating contact is at voltage V_m and temperature T_m, as described in the main text. Current leaves the floating contact via two arms, one of which is partitioned by a QPC en route to the Amp contact. A fictitious floating contact is placed right before the QPC. The fictitious floating contact has a temperature T_{rel}, which represents the effective local temperature of the edge at the point of partitioning, and a voltage V_c, which is determined self-consistently satisfying the demand that no charge accumulates within the contact.

Figure S3. **Partitioned thermal noise measurement methodology** (a) SEM image of the device, DC current with opposite polarity is sourced in S_1 and S_2 giving finite ΔP and $V_m = 0$. Edge modes flowing out from the right side of the small floating contact encounters two QPCs at 20μm and at 140μm away from the small floating contact. Conductance and noise are measured at the amplifier as function of the QPCs split-gate voltage. (b) Differential conductance (also reflection coefficient) of QPC1 and QPC2 as function of V_{QPC1} and V_{QPC2}, measured at v=2 (c) Excess noise as function of the split gate voltage of each QPC at v=2. (d) Normalized noise as function of the reflection of each QPC, rendered from the two plots in (c) and (b).

Figure S4. **Forcing relaxation with cold floating contact. (a)** SEM image of the device, sourcing constant DC current from S_1 and S_2 with opposite polarity in order to heat the small floating contact and leave it with zero voltage. The hot channel is partitioned at QPC1, keeping QPC2 fully pinched, while noise is measured in the amplifier. **(b)** Normalized noise measured ν=2 as function of the reflection of the QPC1 as described in (a). The upper black curve is the non-relaxed limit and the lower black curves are the fully relaxed limit for a single channel. **(c)** Heating the small floating contact with constant DC current sourced from S_1 and S_2 with opposite polarity. The hot channel fully transmits through the first QPC and flows into a massive floating contact, cooling the edge down to base temperature T_0. The channel then flows to the second QPC and partitioned while measuring noise on the amplifier. **(d)** Normalized noise measured at ν =2 as function of the reflection of the second QPC as described in (c). The upper black curve is the non-relaxed limit and the lower black curve is the fully relaxed limit for a single channel.

Figure S5. **Thermal relaxation of edge modes in particle-like states.** Partitioned thermal noise as a function of the reflection coeficient at a constant temperature difference. Green circles – partitioning QPC1 while keeping QPC2 fully pinched; Orange circles - partitioning QPC2 while keeping QPC1 fully pinched. The upper solid line is the no-relaxation limit for $h = 0$, the upper dashed line is the no-relaxation limit when taking into account $h(T_m/T_0)$, the lower dashed line is the full-relaxation limit (doesn't depend on h). Best fit of the relaxation parameter, Θ_1 for QPC1 (green solid line) and Θ_2 for QPC2 (orange solid line), using Eq. 3. **(a)** $\Theta_{1inner} = 1.06$, $\Theta_{1middle} = 1.08$, $\Theta_{1outer} = 1.09$; $\Theta_{2inner} = 1.00$, $\Theta_{2middle} = 0.99$, $\Theta_{2outer} = 0.88$. **(b)** $\Theta_{1inner} = 1.11$, $\Theta_{1middle} = 1.16$, $\Theta_{1outer} = 1.12$; $\Theta_{2inner} = 0.91$, $\Theta_{2middle} = 0.73$, $\Theta_{2outer} = 0.74$. **(c)** $\Theta_{1inner} = 0.92$, $\Theta_{1middle} = 0.9$, $\Theta_{1outer} = 0.85$; $\Theta_{2inner} = 0.42$, middle and outer modes are mixed at QPC2, no fitteing available. **(d)** $\Theta_{1inner} = 1.07$, $\Theta_{1outer} = 0.97$; $\Theta_{2inner} = 0.75$, $\Theta_{2outer} = 0.75$. **(e)** $\Theta_{1inner} = 1.05$, $\Theta_{1outer} = 0.94$; $\Theta_{2inner} = 0.63$, $\Theta_{2outer} = 0.67$. **(f)** $\Theta_{1inner} = 0.70$, $\Theta_{1outer} = 0.62$; $\Theta_{2inner} = 0.31$, $\Theta_{2outer} = 0.38$. **(g)** $\Theta_1 = 1.01$, $\Theta_2 = 0.68$. **(h)** $\Theta_1 = 0.94$, $\Theta_2 = 0.63$. **(i)** $\Theta_1 = 0.8$, $\Theta_2 = 0.46$. **(j)** $\Theta_1 = 0.57$, $\Theta_2 = 0.34$. **(k)** $\Theta_1 = 0.58$, $\Theta_2 = 0.34$.

Figure S6. **Thermal relaxation of edge modes in hole-conjugate states.** Partitioned thermal noise as a function of the reflection coeficient at a constant temperature difference. Green circles – partitioning QPC1 while keeping QPC2 fully pinched; Orange circles - partitioning QPC2 while keeping QPC1 fully pinched. The upper solid line is the no-relaxation limit for $h = 0$, the upper dashed line is the no-relaxation limit when taking into account $h(T_m/T_0)$, the lower dashed line is the full-relaxation limit (doesn't depend on h). Best fit of the relaxation parameter, Θ_1 for QPC1 (green solid line) and Θ_2 for QPC2 (orange solid line), using Eq. 3. **(a)** $\Theta_1 = 0.74, \Theta_2 = 0.49$. **(b)** $\Theta_1 = 0.74, \Theta_2 = 0.49$. **(c)** $\Theta_1 = 0.74, \Theta_2 = 0.47$. **(d)** $\Theta_1 = 0.46, \Theta_2 = 0.24$. **(e)** $\Theta_1 = 0.50, \Theta_2 = 0.24$. **(f)** $\Theta_1 = 0.62, \Theta_2 = 0.39$. **(g)** $\Theta_1 = 0.65, \Theta_2 = 0.37$. **(h)** $\Theta_1 = 0.65, \Theta_2 = 0.35$. **(i)** $\Theta_1 = 0.29, \Theta_2 = 0.10$. **(j)** $\Theta_1 = 0.34, \Theta_2 = 0.10$. **(k)** $\Theta_1 = 0.53, \Theta_2 = 0.26$. **(l)** $\Theta_1 = 0.57, \Theta_2 = 0.25$. **(m)** $\Theta_1 = 0.59, \Theta_2 = 0.28$. **(n)** $\Theta_1 = 0.35, \Theta_2 = 0.15$. **(o)** $\Theta_1 = 0.39, \Theta_2 = 0.15$.

Figure S7. **Calibration of the amplifier. (a)** Shot-noise measurement at $\nu = 2$ for calibration of gain and temperature. **(b)** Thermal noise as function of base temperature of the fridge to verify calibration of gain at $\nu = 2$.